J. Fluid Mech. (1985), *vol.* 150, *pp.* 311–327
Printed in Great Britain

Asynchronous whirl in a rotating cylinder partially filled with liquid

By A. S. BERMAN, T. S. LUNDGREN AND A. CHENG
Department of Aerospace Engineering and Mechanics, University of Minnesota, Minneapolis, Minnesota 55455

(Received 29 December 1983 and in revised form 25 July 1984)

Experimental and analytical results are presented for the self-excited oscillations that occur in a partially filled centrifuge when centrifugal forces interact with shallow-water waves. Periodic and aperiodic modulations of the basic whirl phenomena are both observed and calculated. The surface waves are found to be hydraulic jumps, undular bores or solitary waves.

1. Introduction

Miles & Troesch (1961) have studied surface waves in a rapidly rotating cylinder partially filled with liquid. Kollmann (1962) and Wolf (1968) have reported self-excited asynchronous whirl phenomena resulting from the interaction of the centrifugal forces induced by these waves with the mechanical supports of the system. Hendricks & Morton (1979) have performed a linear stability analysis for this configuration, thus identifying the parameter range where this instability occurs. The present work focuses on nonlinear effects which occur within this parameter range. Both experimental and analytical results are presented.

A model for the phenomena consists of a hollow cylinder of radius R (see figure 1) on an axially symmetric support system consisting of linear springs and dampers. (The actual device is described in detail in §5.) The cylinder contains a relatively small amount of liquid, which, by virtue of large angular velocity ω, is spun up into a thin layer along the cylinder wall. In its unperturbed state the layer is of uniform thickness, and the centre of rotation is at the centre of the cylinder. When the liquid layer is perturbed by surface waves the system becomes unbalanced. In a certain parameter range both the amplitude of the waves and the displacement of the centre of rotation grow until a new equilibrium is reached in which the centre of rotation whirls about a fixed point with constant angular velocity Ω and constant displacement Δ. Since Ω is not equal to ω the phenomenon is called asynchronous whirl. (Synchronous whirl occurs when an unbalancing mass is fixed to the cylinder wall.)

A physical explanation of this phenomenon is quite simple. The rotating layer of liquid feels a centrifugal force $R\omega^2$ per unit mass. This effective gravity allows shallow-water waves with propagation speed $(R\omega^2 h_0)^{\frac{1}{2}}$ to occur, where h_0 is the unperturbed thickness of the layer. Waves propagate with this speed relative to an observer fixed to the cylinder. Relative to such an observer, 'off-centre' unbalance or 'tidal' forces travel around the cylinder with speed $(\Omega-\omega)R$. Resonance will occur when these speeds coincide, since a single surface wave will feel this 'tidal' force continuously. The resonance condition is thus

$$(\Omega-\omega)R = \pm(R\omega^2 h_0)^{\frac{1}{2}}$$

or

$$\Omega = \omega[1-(h_0/R)^{\frac{1}{2}}]. \tag{1.1}$$

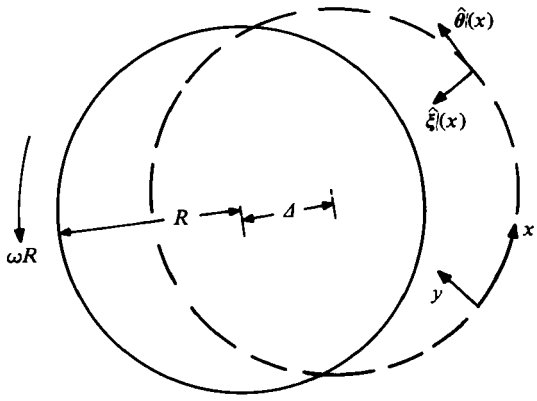

FIGURE 1. Sketch showing some nomenclature; Δ is the amplitude, ω is the operating frequency.

(The other sign is not observed.) The amplitude-response curve (Δ *vs.* ω) would be expected (and is observed) to peak when Ω is near the natural frequency of the elastic support system.

In addition to the basic steady whirl described above, other phenomena are observed and reported here for the first time. In certain parameter ranges Δ is found to oscillate at a frequency that is small compared with Ω, causing a slow modulation of the basic phenomena. In other ranges the modulation is aperiodic. The waves that appear on the water surface are variously hydraulic jumps, undular bores or solitary waves. These can be seen in figures 2(*a*, *b*, *c*), and are further described in §6.

2. Basic equations

The equations of motion of a thin fluid layer along the inside surface of a rotating cylinder, as seen from a coordinate system attached to the cylinder (see figure 1), can be written approximately as

$$\frac{\partial u}{\partial x}+\frac{\partial v}{\partial y}=0, \tag{2.1}$$

$$\frac{\partial u}{\partial t}+u\frac{\partial u}{\partial x}+v\frac{\partial u}{\partial y}-2\omega v+\ddot{\Delta}\cdot\hat{\theta}=-\frac{1}{\rho}\frac{\partial p}{\partial x}+\nu\frac{\partial^2 u}{\partial y^2}, \tag{2.2}$$

$$\frac{\partial v}{\partial t}+2\omega u+R\omega^2=-\frac{1}{\rho}\frac{\partial p}{\partial y}. \tag{2.3}$$

Here, $\Delta(x)$ is the deflection of the centreline of the cylinder from its equilibrium position. The term $\ddot{\Delta}\cdot\hat{\theta}$ appears as a body force in (2.2) because the coordinate frame is being accelerated. A corresponding term has been neglected in (2.3) because the layer is thin; the nonlinear and viscous terms have also been omitted. In addition, v in this equation will be approximated by $v = y(\partial h/\partial t)/h_0$ in the layer, where $h(x,t)$ is the depth and h_0 the mean depth of the layer. These are standard approximations of shallow-water theory (see Whitham 1974). When (2.3) is integrated between y and h, where $p = 0$, one finds

$$\frac{p}{\rho}=\frac{h_0^2-y^2}{2h_0}\frac{\partial^2 h}{\partial t^2}+2\omega\int_y^h u\,\mathrm{d}y+R\omega^2(h-y). \tag{2.4}$$

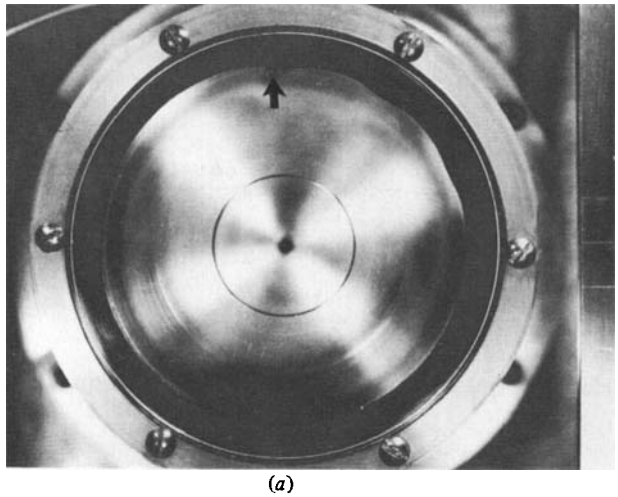

(*a*)

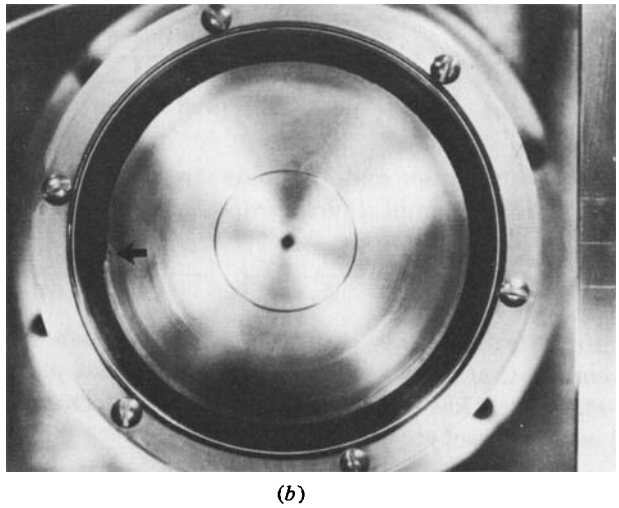

(*b*)

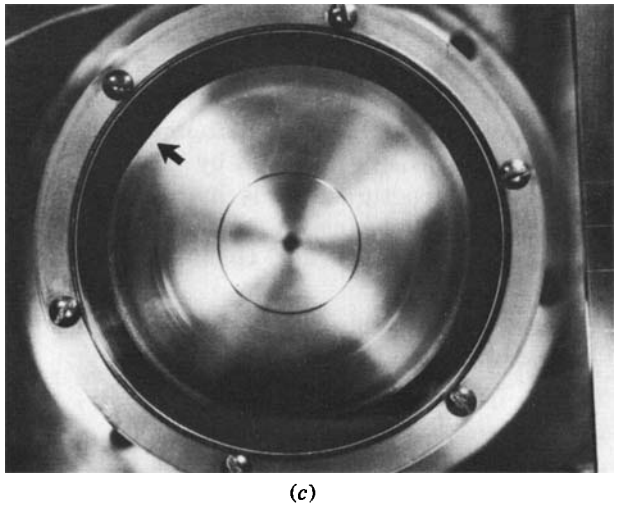

(*c*)

FIGURE 2. Waves on thin liquid layer: (*a*) undular bore; (*b*) hydraulic jump; (*c*) solitary wave.

Differentiating this with respect to x, using (2.1) and the surface boundary condition $\partial h/\partial t + u\,\partial h/\partial x = v$ at $y = h$, and substituting into (2.2) gives

$$\frac{\partial u}{\partial x} + \frac{\partial v}{\partial y} = 0, \tag{2.5}$$

$$\frac{\partial u}{\partial t} + u\frac{\partial u}{\partial x} + v\frac{\partial u}{\partial y} + \ddot{\boldsymbol{\Delta}}\cdot\hat{\boldsymbol{\theta}} = -R\omega^2\frac{\partial h}{\partial x} + 2\omega\frac{\partial h}{\partial t} - \frac{1}{2}\frac{h_0^2 - y^2}{h_0}\frac{\partial^3 h}{\partial x\,\partial t^2} + \nu\frac{\partial^2 u}{\partial y^2}. \tag{2.6}$$

These will be put in the form of depth-averaged equations used in hydraulics. By introducing

$$U = \frac{1}{h}\int_0^h u\,\mathrm{d}y \tag{2.7}$$

and using the surface boundary condition, the following equations may be derived:

$$\frac{\partial h}{\partial t} + \frac{\partial hU}{\partial x} = 0, \tag{2.8}$$

$$\begin{aligned}\frac{\partial U}{\partial t} + U\frac{\partial U}{\partial x} + \ddot{\boldsymbol{\Delta}}\cdot\hat{\boldsymbol{\theta}} = {} & -R\omega^2\frac{\partial h}{\partial x} \\ & + 2\omega\frac{\partial h}{\partial t} \qquad -\tfrac{1}{3}h_0\frac{\partial^3 h}{\partial x\,\partial t^2} \qquad -\frac{\nu}{h_0}\frac{\partial u}{\partial y}\bigg|_{y=0} \qquad -\frac{\partial}{\partial x}\frac{1}{h_0}\int_0^{h_0}(u-U)^2\,\mathrm{d}y. \\ & \text{(Coriolis force)} \quad \text{(dispersion term)} \quad \text{(wall friction)} \quad \text{(Reynolds stress)}\end{aligned} \tag{2.9}$$

In these equations the wall-friction and Reynolds-stress terms must be approximated. The wall friction has been taken in a form proposed by Chester (1968), namely

$$f = -\frac{\nu}{h_0}\frac{\partial u}{\partial y}\bigg|_{y=0} = -\frac{1}{h_0}\left(\frac{\nu}{\pi}\right)^{\frac{1}{2}}\int_0^{\infty}\frac{\partial U(t-t',x)}{\partial t}\frac{\mathrm{d}t'}{(t')^{\frac{1}{2}}}. \tag{2.10}$$

This form is appropriate for steady-state operation in which the motion in a thin viscous layer resembles that generated by an oscillating flat plate.

The Reynolds-stress term has been approximated by using a spatially constant (but time-dependent) eddy viscosity:

$$g = -\frac{\partial}{\partial x}\frac{1}{h_0}\int_0^{h_0}(u-U)^2\,\mathrm{d}y = \frac{\partial}{\partial x}\nu_{\mathrm{T}}\frac{\partial U}{\partial x}, \tag{2.11}$$

$$\nu_{\mathrm{T}} = ah_0^{\frac{3}{2}}\left[\frac{1}{2\pi}\int_0^{2\pi R}\left(\frac{\partial U}{\partial x}\right)^2\mathrm{d}x\right]^{\frac{1}{2}}. \tag{2.12}$$

This term accounts for turbulence which develops in the observed hydraulic jumps. It becomes important only when the velocity gradient becomes large. Equation (2.12) is a modification of an eddy viscosity proposed by Whitham (1974). An alternative approach is to neglect the structure of this hydraulic jump and treat it as a discontinuity as in §3. In §4 the system of equations is solved by expanding in a Fourier series. This requires a 'realistically' thick hydraulic jump for convergence reasons.

It is tempting to neglect the Coriolis-acceleration term. It is shown here that it is important. Consider the linearized equations

$$\frac{\partial h'}{\partial t} + h_0\frac{\partial U}{\partial x} = 0, \tag{2.13}$$

$$\frac{\partial U}{\partial t} + R\omega^2\frac{\partial h'}{\partial x} - 2\omega\frac{\partial h'}{\partial t} = 0, \tag{2.14}$$

where $h = h_0 + h'$. These equations have solutions in the form of the superposition of prograde (faster than the wall) and retrograde waves:

$$F_1(x - c_+ t) + F_2(x - c_- t). \tag{2.15}$$

The wave speeds are

$$c_\pm = R\omega\left[\frac{h_0}{R} \pm \left[\frac{h_0}{R} + \left(\frac{h_0}{R}\right)^2\right]^{\frac{1}{2}}\right]. \tag{2.16}$$

These are in agreement with the two-dimensional results of Miles & Troesch (1961) for shallow water. If the Coriolis acceleration were neglected these would become

$$c_\pm = \pm c_0, \quad c_0 = R\omega\left(\frac{h_0}{R}\right)^{\frac{1}{2}}, \tag{2.17}$$

where c_0 is the shallow-water wave speed $(gh_0)^{\frac{1}{2}}$, with g replaced by the centrifugal acceleration $R\omega^2$. Clearly the Coriolis force would be negligible if h_0/R were sufficiently small. However for $h_0/R = 0.1$ one gets $c_+/c_0 = 1.365$, $c_-/c_0 = -0.733$, which is an appreciable effect. Larger values of h_0/R are used in some of the experiments.

The fluid motion is coupled to the elastic support system by the following combined momentum equation:

$$M\ddot{\Delta} + \frac{\mathrm{d}}{\mathrm{d}t}(\text{the momentum of the fluid}) + 2M\omega_0 C\dot{\Delta} + M\omega_0^2 \Delta = 0. \tag{2.18}$$

Here M is the mass per unit length of the support system, C a dimensionless damping coefficient and ω_0 the natural frequency of the spring system. This may be written

$$(M+m)\ddot{\Delta} + 2M\omega_0 C\dot{\Delta} + M\omega_0^2 \Delta = -\frac{\mathrm{d}}{\mathrm{d}t}\int_0^{2\pi R} \rho h(U + R\omega)\hat{\boldsymbol{\theta}}\,\mathrm{d}x. \tag{2.19}$$

By representing the displacement vector Δ in the form

$$\Delta = \hat{\imath}\Delta\cos\gamma + \hat{\jmath}\Delta\sin\gamma, \tag{2.20}$$

(2.19) may be written as the pair

$$\begin{aligned}(M+m)(\ddot{\Delta} - \Delta\dot{\gamma}^2) + 2M\omega_0 C\dot{\Delta} + M\omega_0^2\Delta \\ = \frac{\mathrm{d}}{\mathrm{d}t}\int_0^{2\pi R} \rho h(U+R\omega)\sin\left(\frac{x}{R} + \omega t - \gamma\right)\mathrm{d}x \\ + \dot{\gamma}\int_0^{2\pi R} \rho h(U+R\omega)\cos\left(\frac{x}{R} + \omega t - \gamma\right)\mathrm{d}x\end{aligned} \tag{2.21}$$

and

$$\begin{aligned}(M+m)(2\dot{\Delta}\dot{\gamma} + \Delta\ddot{\gamma}) + 2M\omega_0 C\Delta\dot{\gamma} \\ = -\frac{\mathrm{d}}{\mathrm{d}t}\int_0^{2\pi R} \rho h(U+R\omega)\cos\left(\frac{x}{R} + \omega t - \gamma\right)\mathrm{d}x \\ + \dot{\gamma}\int_0^{2\pi R} \rho h(U+R\omega)\sin\left(\frac{x}{R} + \omega t - \gamma\right)\mathrm{d}x.\end{aligned} \tag{2.22}$$

The above system of coupled equations may be greatly simplified in the case where the mass per unit length of the support system (M) is much greater than the mass per unit length of the fluid (m), for in this case the magnitude of the unstable oscillations will be small. The mass parameter

$$\mu = \frac{\pi\rho R^2}{M} \tag{2.23}$$

is introduced along with new variables defined by

$$\left.\begin{aligned} \frac{\Delta}{h_0} &= \mu^2\tilde{\Delta}, \quad \frac{fR}{c_0^2} = \mu^2\tilde{f}, \quad \frac{gR}{c_0^2} = \mu^2\tilde{g}, \\ \frac{U}{c_0} &= \mu\tilde{U}, \quad \frac{h'}{h_0} = \mu\tilde{h}, \quad \frac{\Omega}{\omega} = \tilde{\Omega}, \end{aligned}\right\} \tag{2.24}$$

where $\Omega = \dot{\gamma}$ and c_0 is the wave speed previously defined. In addition a new x-variable is defined by

$$\zeta = x/R + \omega t - \gamma(t) \tag{2.25}$$

and a slow time by

$$\tau = \mu\omega(h_0/R)^{\frac{1}{2}}t. \tag{2.26}$$

In the new variables the 'tidal' driving term appears stationary with slowly varying magnitude. It is assumed that all the variables depend only on the slow time τ and not additionally on a fast time ωt. This means that the motion is nearly synchronized to the driving wave with time variations which are slow compared to the turnaround period of the cylinder.

With the above change of variables the equations may be written

$$\left(\frac{R}{h_0}\right)^{\frac{1}{2}}(1-\tilde{\Omega})\frac{\partial\tilde{h}}{\partial\zeta} + \frac{\partial\tilde{U}}{\partial\zeta} = \mu G_1, \tag{2.27}$$

$$\left(\frac{R}{h_0}\right)^{\frac{1}{2}}(1-\tilde{\Omega})\frac{\partial\tilde{U}}{\partial\zeta} + \frac{\partial\tilde{h}}{\partial\zeta} - 2(1-\tilde{\Omega})\frac{\partial\tilde{h}}{\partial\zeta} = \mu G_2, \tag{2.28}$$

where

$$G_1 = -\frac{\partial\tilde{h}}{\partial\tau} - \frac{\partial\tilde{h}\tilde{U}}{\partial\zeta} \tag{2.29}$$

and

$$G_2 = -\frac{\partial\tilde{U}}{\partial\tau} - \tilde{U}\frac{\partial\tilde{U}}{\partial\zeta} + \left(\mu^2\frac{h_0}{R}\tilde{\Delta}'' - \tilde{\Delta}\tilde{\Omega}^2\right)\sin\zeta - \mu\left(\frac{h_0}{R}\right)^{\frac{1}{2}}(2\tilde{\Delta}'\tilde{\Omega} + \tilde{\Omega}')\cos\zeta$$
$$+ 2\left(\frac{h_0}{R}\right)^{\frac{1}{2}}\frac{\partial\tilde{h}}{\partial\tau} - \frac{1}{3}\frac{h_0^2}{\mu R^2}\frac{\partial}{\partial\zeta}\left[\mu\frac{\partial}{\partial\tau} + \left(\frac{R}{h_0}\right)^{\frac{1}{2}}(1-\tilde{\Omega})\frac{\partial}{\partial\zeta}\right]^2\tilde{h} + \tilde{f}, \tag{2.30}$$

where the prime refers to differentiation with respect to the slow time. Now expand in a power series in μ,

$$\left.\begin{aligned} \tilde{U} &= \tilde{U}_0 + \mu\tilde{U}_1 + \ldots, \quad \tilde{h} = H + \mu\tilde{h}_1 + \ldots, \quad \tilde{\Delta} = \tilde{\Delta}_0 + \mu\tilde{\Delta}_1 + \ldots, \\ \tilde{\Omega} &= \tilde{\Omega}_0 + \mu\tilde{\Omega}_1 + \ldots, \quad G_1 = G_{10} + \mu G_{11} + \ldots, \quad G_2 = G_{20} + \mu G_{21} + \ldots, \end{aligned}\right\} \tag{2.31}$$

and assume that the factor $h_0^2/\mu R^2$ in the dispersion term is $O(1)$ for purposes of expansion. The lowest terms in the expansion give

$$\left(\frac{R}{h_0}\right)^{\frac{1}{2}}(1-\tilde{\Omega}_0)\frac{\partial H}{\partial\zeta} + \frac{\partial\tilde{U}_0}{\partial\zeta} = 0, \tag{2.32}$$

$$\left(\frac{R}{h_0}\right)^{\frac{1}{2}}(1-\tilde{\Omega}_0)\frac{\partial\tilde{U}_0}{\partial\zeta} + \frac{\partial H}{\partial\zeta} - 2(1-\tilde{\Omega}_0)\frac{\partial H}{\partial\zeta} = 0. \tag{2.33}$$

These can only have a solution if

$$1-\tilde{\Omega}_0 = -\frac{h_0}{R} \pm \left[\frac{h_0}{R} + \left(\frac{h_0}{R}\right)^2\right]^{\frac{1}{2}}. \tag{2.34}$$

With the plus sign this gives

$$\tilde{\Omega}_0 = 1 + \frac{c_-}{\omega R}, \tag{2.35}$$

that is,

$$R\Omega_0 = \omega R + c_-. \tag{2.36}$$

Thus to lowest order the whirl speed is synchronized with retrograde water waves relative to the cylinder surface velocity. The other sign would lead to prograde waves. This choice is rejected as non-physical. With the above choice for $\tilde{\Omega}_0$, either of the equations give

$$\tilde{U}_0 = \frac{c_-}{c_0} H. \tag{2.37}$$

The next term in the expansion gives

$$\frac{\partial \tilde{U}_1}{\partial \zeta} - \frac{c_-}{c_0}\frac{\partial \tilde{h}_1}{\partial \zeta} = G_{10} + \left(\frac{R}{h_0}\right)^{\frac{1}{2}} \tilde{\Omega}_1 \frac{\partial H}{\partial \zeta}, \tag{2.38}$$

$$\frac{\partial \tilde{U}_1}{\partial \zeta} - \frac{c_-}{c_0}\frac{\partial \tilde{h}_1}{\partial \zeta} = -\frac{c_0}{c_-}\left[G_{20} + \left(\frac{R}{h_0}\right)^{\frac{1}{2}} \tilde{\Omega}_1 \frac{\partial \tilde{U}_0}{\partial \zeta} - 2\tilde{\Omega}_1 \frac{\partial H}{\partial \zeta}\right]. \tag{2.39}$$

A necessary condition for these to have a solution is for the right-hand sides to be equal:

$$G_{10} + \left(\frac{R}{h_0}\right)^{\frac{1}{2}} \tilde{\Omega}_1 \frac{\partial H}{\partial \zeta} = -\frac{c_0}{c_-}\left[G_{20} + \left(\frac{R}{h_0}\right)^{\frac{1}{2}} \tilde{\Omega}_0 \frac{\partial \tilde{U}_0}{\partial \zeta} - 2\tilde{\Omega}_1 \frac{\partial H}{\partial \zeta}\right]. \tag{2.40}$$

An additional condition is required because the solution must be periodic. This requires that the average of the right-hand sides must be zero. This condition is satisfied if

$$\int_0^{2\pi} \tilde{f}\, \mathrm{d}\zeta = 0.$$

The expression for $\tilde{f}$ given by (2.10) or (2.42) satisfies this condition.

When $\tilde{U}_0$ from (2.37) is substituted into (2.40) a modified, driven, Korteweg–de Vries equation for H results, namely

$$\frac{\partial H}{\partial \tau_1} + A_1 \frac{\partial H}{\partial \zeta} - B_1 H \frac{\partial H}{\partial \zeta} - C_1 \frac{\partial^3 H}{\partial \zeta^3} + \tilde{f} + \tilde{g} = \tilde{\Delta}_0 \tilde{\Omega}_0^2 \sin\zeta. \tag{2.41}$$

Here

$$\tau_1 = \tau \frac{\left(\frac{h_0}{R}\right)^{\frac{1}{2}}}{2\left[\frac{h_0}{R} + \left(\frac{h_0}{R}\right)^2\right]^{\frac{1}{2}}}, \quad A_1 = \frac{-2\tilde{\Omega}_1\left[\frac{h_0}{R} + \left(\frac{h_0}{R}\right)^2\right]^{\frac{1}{2}}}{\left(\frac{h_0}{R}\right)^{\frac{1}{2}}}, \quad B_1 = 3\left(\frac{c_-}{c_0}\right)^2,$$

$$C_1 = \frac{1}{3}\frac{h_0^2}{\mu R^2}\left(\frac{c_-}{c_0}\right)^2, \quad \frac{c_-}{c_0} = \frac{\frac{h_0}{R} - \left[\frac{h_0}{R} + \left(\frac{h_0}{R}\right)^2\right]^{\frac{1}{2}}}{\left(\frac{h_0}{R}\right)^{\frac{1}{2}}}, \quad \tilde{\Omega}_0 = 1 + \frac{c_-}{\omega R}.$$

The wall-friction term $\tilde{f}$ may be expressed as

$$\tilde{f} = D_1 \int_0^{\infty} \frac{\partial H(\zeta - \zeta', \tau_1)}{\partial \zeta} \frac{\mathrm{d}\zeta'}{\zeta'^{\frac{1}{2}}}, \quad D_1 = \frac{1}{\pi^{\frac{1}{2}}} \frac{\left(\frac{\nu}{\omega R^2}\right)^{\frac{1}{2}} \left(\frac{c_-}{c_0}\right)^2}{\mu \left(\frac{h_0}{R}\right)^{\frac{5}{4}}} \tag{2.42}$$

and the Reynolds-stress term $\tilde{g}$ as

$$\tilde{g} = -E_1 \frac{\partial^2 H}{\partial \zeta^2}, \quad E_1 = a\left(\frac{h_0}{R}\right)^{\frac{3}{2}}\left(\frac{c}{c_0}\right)^2\left[\frac{1}{2\pi}\int_0^{2\pi}\left(\frac{\partial H}{\mathrm{d}\zeta}\right)^2 \mathrm{d}\zeta\right]^{\frac{1}{2}}. \tag{2.43}$$

The same expansion applied to the rotor equations reduces them to

$$\tilde{A}_0\left(\frac{\omega_0^2}{\omega^2} - \tilde{\Omega}_0^2\right) = \tilde{\Omega}_0^2 \frac{1}{\pi}\int_0^{2\pi} H \cos\zeta \, \mathrm{d}\zeta \tag{2.44}$$

and

$$\tilde{A}_0 \frac{\omega_0}{\omega}\tilde{\Omega}_0 C = \tilde{\Omega}_0^2 \frac{1}{\pi}\int_0^{2\pi} H \sin\zeta \, \mathrm{d}\zeta. \tag{2.45}$$

It is desired to solve (2.41) for $H(\zeta, \tau_1)$ with period 2π and zero average. This equation contains two unknown functions, $\tilde{A}_0(\tau_1)$ and $A_1(\tau_1)$, which must be determined by using the two constraining equations (2.44) and (2.45).

3. The hydraulic-jump approximation

In this section a simplified nonlinear analysis is carried out. It is assumed that the oscillations are steady. The dispersion term and the wall-friction term are neglected as is the Reynolds-stress term. A solution is sought which may have a discontinuity in depth (a hydraulic jump). Equation (2.41) then reduces to

$$A_1 \frac{\partial H}{\partial \zeta} - B_1 H \frac{\partial H}{\partial \zeta} = \tilde{\Omega}_0^2 \tilde{A}_0 \sin\zeta, \tag{3.1}$$

which may be integrated to

$$A_1 H - \tfrac{1}{2} B_1 H^2 = -\tilde{\Omega}_0^2 \tilde{A}_0 \cos\zeta + A, \tag{3.2}$$

where A is a constant of integration. When solved for H this gives two solutions:

$$H = \frac{A_1}{B_1} \pm \left[\left(\frac{A_1}{B_1}\right)^2 - \frac{2(A - \tilde{\Omega}_0^2 \tilde{A}_0 \cos\zeta)}{B_1}\right]^{\frac{1}{2}}. \tag{3.3}$$

These are sketched in figure 3(*a*). A hydraulic jump may be represented by a jump from the lower branch to the upper branch. However, since H must be periodic, this requires that the two branches touch at $\zeta = \pm\pi$. This may be accomplished by choosing the constant A so that

$$(A_1/B_1)^2 = 2(A + \tilde{\Omega}_0^2 \tilde{A}_0)/B_1. \tag{3.4}$$

Then H is given by

$$H = \frac{A_1}{B_1} \pm \left(\frac{2\tilde{\Omega}_0^2 \tilde{A}_0}{B_1}\right)^{\frac{1}{2}} (1 + \cos\zeta)^{\frac{1}{2}}. \tag{3.5}$$

This is sketched in figure 3(*b*) along with a possible jump at $\zeta = S$.

The solution is therefore given by (3.5) with three unknown parameters, A_1, $\tilde{A}_0$ and the unknown jump location S. In addition to the two integral constraints given by (2.44) and (2.45), a third constraint is provided by conservation of mass:

$$\int_{-\pi}^{\pi} H \, \mathrm{d}\zeta = 0. \tag{3.6}$$

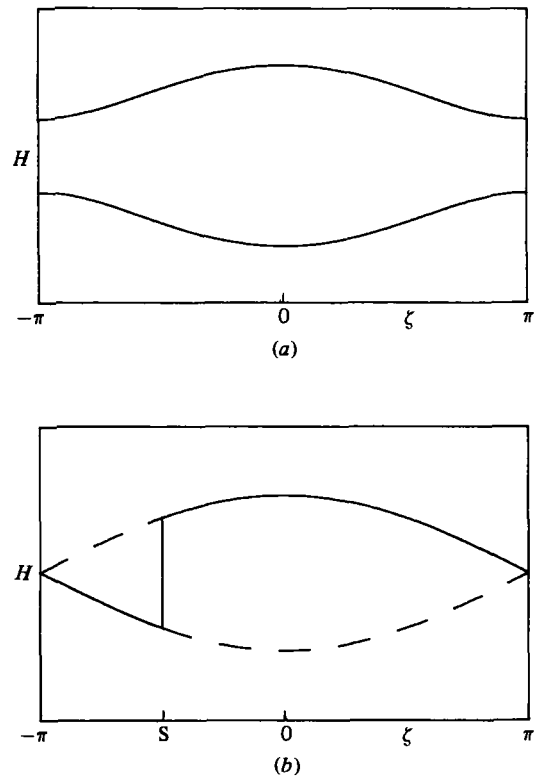

FIGURE 3. Depth variation in hydraulic-jump approximation: (*a*) two possible solutions; (*b*) limiting case with jump at S.

This may be regarded as determining the constant A_1, while the other two determine $\bar{\Delta}_0$ and S. The integrations in (2.44) and (2.45) may be carried out with the results

$$\bar{\Delta}_0^{\frac{1}{2}}\left(\frac{\omega_0^2}{\omega^2}-\bar{\Omega}_0^2\right)=-\bar{\Omega}_0^3\left(\frac{2}{B_1}\right)^{\frac{1}{2}}\frac{4(2)^{\frac{1}{2}}}{\pi}(\sin\tfrac{1}{2}S-\tfrac{2}{3}\sin^3\tfrac{1}{2}S), \tag{3.7}$$

$$\bar{\Delta}_0^{\frac{1}{2}}\frac{\omega_0}{\omega}\bar{\Omega}_0 C=\bar{\Omega}_0^3\left(\frac{2}{B_1}\right)^{\frac{1}{2}}\frac{4}{3\pi}(1+\cos S)^{\frac{3}{2}}. \tag{3.8}$$

An equation for S alone is obtained by dividing out $\bar{\Delta}_0^{\frac{1}{2}}$, giving

$$\frac{2\omega_0^2/\omega^2-\bar{\Omega}_0^2}{(\omega_0/\omega)\bar{\Omega}_0 C}=-3(2)^{\frac{1}{2}}\frac{2[\sin\frac{1}{2}S-\frac{2}{3}\sin^3\frac{1}{2}S]}{(1+\cos S)^{\frac{3}{2}}}. \tag{3.9}$$

The jump position versus ω/ω_0 may be determined from the inverse function, specifying S and determining ω/ω_0. Then with S known $\bar{\Delta}_0$ may be found from (3.7) or (3.8).

Results are plotted in figure 4 as Δ_0/h_0 versus ω/ω_0 for one particular set of centrifuge parameters, $h_0/R = 0.14$ and $C = 0.18$. The peak in this curve is fairly sensitive to the value of the damping, as with most amplitude-response curves. A 10 % change in the damping has about a 20 % effect on the peak amplitude, while hardly changing the tails of this curve. It will be observed that this result is in remarkably good agreement with the more exact theory and the experiments, considering the simple nature of the theory.

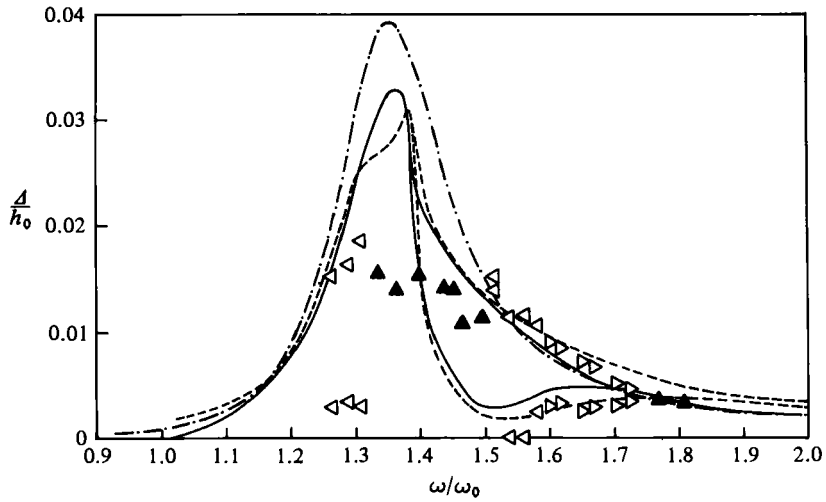

FIGURE 4. Amplitude versus operating frequency for $h_0/R = 0.14$, $C = 0.18$, $\mu = 0.032$: –·–·–·, hydraulic jump approximation; ——, modified Korteweg–de Vries equation, $E_1 = 0.0015$; – – – –, modified Korteweg–de Vries equation, $E_1 = 0$; ▷, experimental, periodic modulation; ◁, experimental, aperiodic modulation; ▲, experimental, steady whirl.

4. Numerical solution of the inhomogeneous Korteweg–de Vries equation

The equations derived in §2 have been expressed as a system of ordinary differential equations by expanding in a Fourier series and truncating at a finite number of terms. The resulting equations for the time-dependent Fourier coefficients have been solved numerically as an initial-value problem. By introducing

$$H = \sum_{n=-\infty}^{\infty} Z_n(\tau_1)\, e^{in\zeta}, \quad Z_{-n} = Z_n^* \tag{4.1}$$

the equations may be written, for $n = 1, 2, 3, \ldots$,

$$\frac{dZ_n}{d\tau_1} = -inA_1 Z_n - in^3 C_1 Z_n - (1+i) D_1 (\tfrac{1}{2}\pi)^{\frac{1}{2}} n^{\frac{1}{2}} Z_n - E_1 n^2 Z_n - \tfrac{1}{2} i \tilde{\Omega}_0^2 \tilde{A}_0 \delta_{1n}$$
$$+ \tfrac{1}{2} inB_1 \left(\sum_{j=1}^{n-1} Z_j Z_{n-j} + \sum_{j=n+1}^{\infty} Z_j Z_{j-n}^* + \sum_{j=1}^{\infty} Z_j^* Z_{n+j} \right), \tag{4.2}$$

where δ_{1n} is the Kronecker delta. The two integral constraints, (2.44) and (2.45), may be combined into a single complex expression,

$$\left(\frac{\omega_0^2}{\omega^2} - \tilde{\Omega}_0^2 - i \frac{\omega_0}{\omega} \tilde{\Omega}_0 C \right) \tilde{A}_0 = 2\tilde{\Omega}_0^2 Z_1, \tag{4.3}$$

which is needed to determine A_1 and $\tilde{A}_0$. By noting that this implies

$$\mathrm{Im}\,(GZ_1) = 0 \tag{4.4}$$

with

$$G = \frac{\omega_0^2}{\omega^2} - \tilde{\Omega}_0^2 + i \frac{\omega_0}{\omega} \tilde{\Omega}_0 C, \tag{4.5}$$

the parameter A_1 may be determined from the first of (4.2), the $n = 1$ equation, by multiplying it by G and taking the imaginary part. This gives

$$A_1 = -C_1 - D_1(\tfrac{1}{2}\pi)^{\frac{1}{2}} + B_1 \frac{\operatorname{Im}\left(\mathrm{i}G \sum_{j=1}^{\infty} Z_j^* Z_{j+1}\right)}{\operatorname{Im}(\mathrm{i}GZ_1)} - \tfrac{1}{2}\bar{\Omega}_0^2 \bar{\Delta}_0 \frac{\operatorname{Im}(\mathrm{i}G)}{\operatorname{Im}(\mathrm{i}GZ_1)}. \tag{4.6}$$

Since $\bar{\Delta}_0$ may be found from

$$\bar{\Delta}_0 = 2\frac{\omega}{\omega_0}\frac{\bar{\Omega}_0 \operatorname{Im}(Z_1)}{C}, \tag{4.7}$$

all the terms on the right-hand side of (4.2) are known in terms of the Z_n. It should be noted, in this regard, that

$$E_1 = a\left(\frac{h_0}{R}\right)^{\frac{3}{2}}\left(\frac{c_-}{c_0}\right)^2\left[2\sum_{j=1}^{\infty} j^2 Z_j Z_j^*\right]. \tag{4.8}$$

The resulting equations have been truncated at 20 terms and solved numerically by using a fourth-order Runge–Kutta algorithm in complex form. There are some complications, however. The terms $-\mathrm{i}n^3 C_1 Z_n$ and $-E_1 n^2 Z_n$ become large when n is large and cause numerical instability unless the time step is very small. The system of equations is 'stiff'. The difficulty can be eliminated by a change of variables. If the equations are written

$$\frac{\mathrm{d}Z_n}{\mathrm{d}\tau_1} = (-\mathrm{i}n^3 C_1 - n^2 E_1) Z_n + F_n \tag{4.9}$$

the use of an integrating factor results in

$$\frac{\mathrm{d}}{\mathrm{d}\tau_1} Z_n I_n = I_n F_n, \tag{4.10}$$

with

$$I_n = \exp\left(-\mathrm{i}n^3 C_1 \tau_1 - n^2 \int_0^{\tau_1} E_1(\tau_1')\,\mathrm{d}\tau_1'\right). \tag{4.11}$$

When a new variable

$$Y_n = Z_n I_n \tag{4.12}$$

is introduced, the new system is not stiff. Convergence is adequate with $\Delta\tau_1 = 0.01$, compared with $\Delta\tau_1 = 10^{-4}$ required before the transformation.

Computations have been carried out for an extended range of operating frequencies with parameters that correspond to a load of 175 cm^3 of water. The parameters used were

$$\left.\begin{gathered}\frac{h_0}{R} = 0.14, \quad \left(\frac{\nu}{\omega_0 R^2}\right)^{\frac{1}{2}} = 0.0015, \quad C = 0.18, \\ \mu = 0.032, \quad a = 0.2.\end{gathered}\right\} \tag{4.13}$$

The computations were carried out for 24 time units starting from an initial state in which only the $n = 1$ coefficients were excited, with the constraint given by (4.4) satisfied. Usually $\operatorname{Im} Z_1 = -0.1$ was used. The results are presented as the amplitude of the rotor oscillation Δ_0/h_0 versus the operating frequency ω/ω_0 in figure 4. For some values of the operating frequency the amplitude rapidly settles down (usually 6 time units) to steady-state oscillation. For a large range of operating frequencies the device does not oscillate at a single frequency but shows modulation of the normal high-frequency oscillations by a slow breathing phenomenon. In the figure this is indicated by showing a maximum and a minimum amplitude. The frequency of the

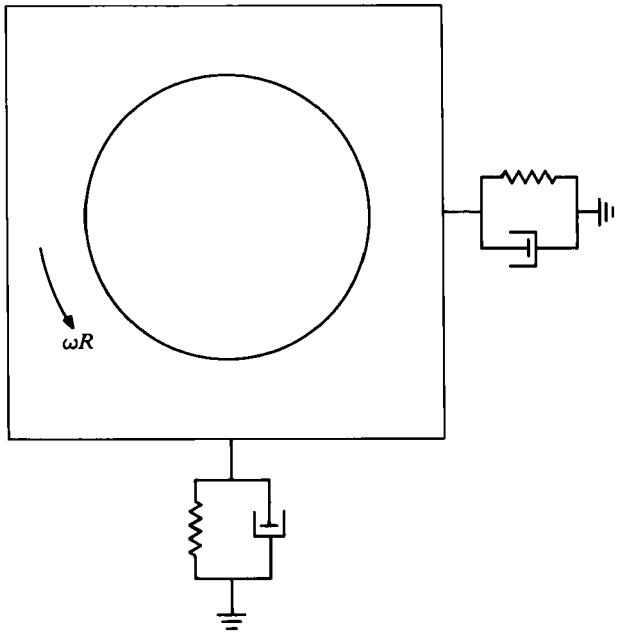

FIGURE 5. Schematic of centrifuge.

slow modulation is of order 1, showing that the scaling used in the equations is correct. No aperiodicities were observed in these computations. However, at a larger external damping, with $C = 0.3$, clear aperiodic phenomena were seen. This will be discussed later.

5. Description of the experiments

The equipment is shown schematically in figure 5. The centrifuge consists of a thick-walled lucite cylinder with O-ring-sealed top and bottom lucite flange plates. The top-plate has a central hole for adding or removing fluid from the centrifuge. The centrifuge bowl is 6 cm in height and has an inner radius of 6 cm. The bowl is kept short to minimize thickness variation in the spun-up liquid layer. The centrifuge is mounted on an aluminium plate, which, with the use of two sets of linear bearings, is free to move in two mutually perpendicular directions. Its motion in these directions is resisted by two adjustable double-cantilever steel springs and is damped by two attached hypodermic syringes filled with silicone oil and connected through variable-length tubing to oil reservoirs.

When the centrifuge is in pure rotation about its geometric axis the aluminium plate is stationary. Any motion of the centrifuge from its equilibrium centred position causes motion of the mounting plate and of the motor driving the bowl. The mechanical ground for the system is a steel plate (about 5 cm thick) mounted firmly to a concrete pier which is part of the building foundation. This eliminates any interaction between the rotating, vibrating system and the surroundings.

The overall design of the equipment is such that the spring constants and damping factors for the two degrees of freedom can be matched closely. In addition, a brass plate, provided with its own set of linear bearings, is built into the system in such a way as to assure that the mass is the same for motion in each of the two directions. The total mass of the vibrating system is about 20 kg. The effective length of the

cantilever springs is variable so that the natural frequency of the system can be changed. These were adjusted so that it was 1100–1200 r.p.m. in most of the experiments. By changing the length of the damper tubing, or the viscosity of the oil in the dampers, the damping coefficient can be varied from about 0.12 to 0.30.

The centrifuge is driven by an Electrocraft feedback-controlled motor which can drive the loaded bowl to about 3000 r.p.m. and can maintain the speed to about ± 1 r.p.m.

The lower flange cover of the bowl is held to the bowl flange by six steel bolts. A Bentley proximity probe mounted at a suitable distance from these bolts senses their passage and trasnsmits 6 pulses per bowl revolution to a counter, which in turn displays the bowl speed when gated for known intervals. If the gate time is 10 s the counter displays the bowl speed in r.p.m.

Motion of the system in the two independent directions is sensed by Kaman proximity probes, which have been calibrated in place and have a sensitivity of about 80 mV/mm and a frequency response from zero to about 20 kHz. The outputs of the Kamen probes are fed to an oscilloscope and to a Hewlett-Packard Model 3502A dual-channel spectrum analyser. This instrument continuously samples a controllable time segment of the signal from the Kamen probes, performs a fast-Fourier-transform analysis and displays the spectrum of the incoming signal. Either r.m.s.-averaged or peak-averaged amplitudes are displayed as a function of frequency. The spectrum analyser communicates with an HP-85 digital computer which controls the analyser operation and receives the spectral data which is stored on magnetic tape for further analysis.

The following is an outline of the procedure used in a typical whirl experiment.

1. The empty centrifuge is unbalanced by attaching a 5 g weight to one of the six screws in the bottom flange. This unbalance produces a synchronous runout. Suitable measurements of the amplitude and phase of this runout provide the data for determining the resonant frequency and damping coefficient associated with the two degrees of freedom of the system. The unbalance weight is removed.

2. The centrifuge is loaded with the desired amount of working fluid whose viscosity and density have been determined. Temperature is measured before and after each whirl run and the fluid properties are taken to be those at the average temperature. Usually the temperature changes by less than about 1 °C during a run.

3. The centrifuge is spun up to the desired speeds and the whirl amplitudes are obtained from the computer, which interrogates the spectrum analyser. The operating speed at which each whirl amplitude is measured is obtained from the digital counter mentioned previously.

4. When the desired range of operating speeds has been covered, and whirl measurements made with both increasing and decreasing operating speed, the run is complete.

5. Measurements of the resonant frequencies and the damping coefficients are repeated.

Visualization of the free surface of the spun-up liquid film is achieved by the addition of a small amount of dye to the fluid and the use of stroboscopic lighting triggered by the Kamen probes which are responding to the whirl. Photographs of the free surface are obtained by synchronized flash photography using a precision Wista view camera.

In some cases, the Kamen probe output was fed, after suitable known amplification, to a Hewlett-Packard hot-stylus recorder. This provided a hard-copy record of the time dependence of whirl amplitude.

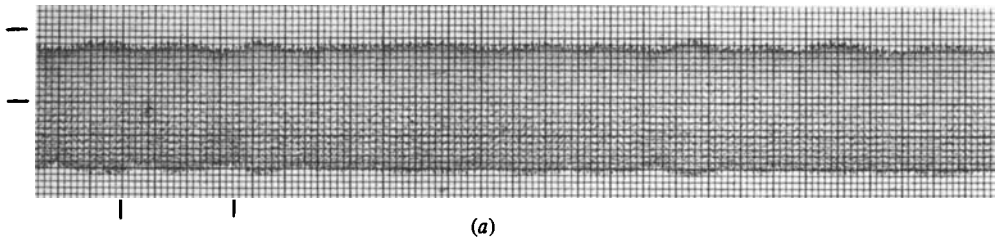

(a)

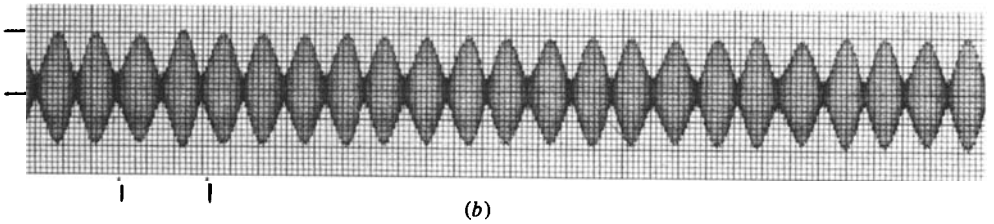

(b)

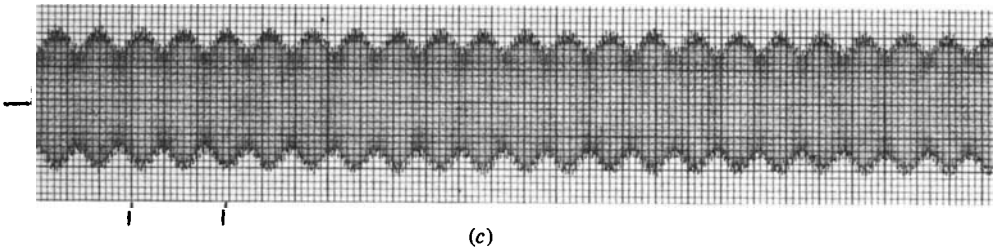

(c)

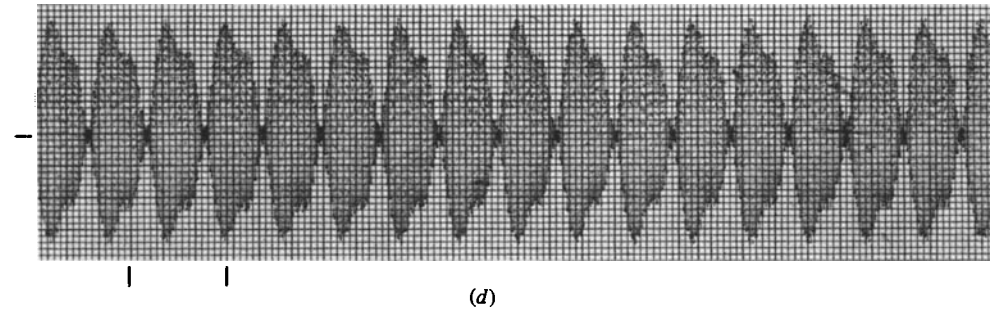

(d)

FIGURE 6. For caption see opposite.

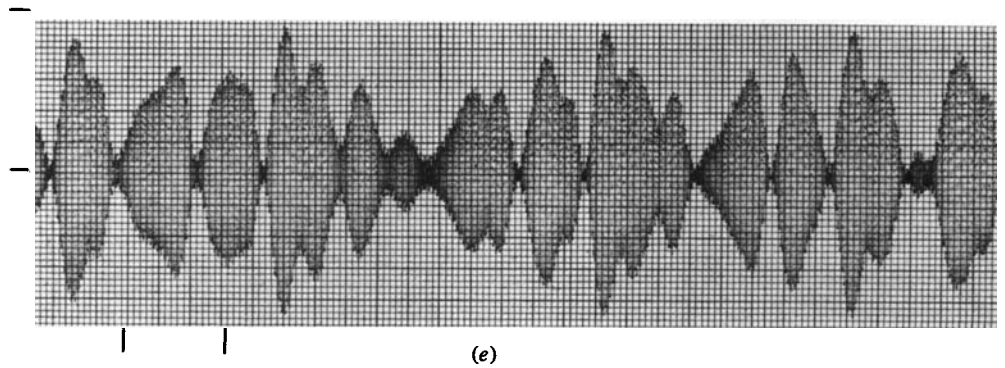

(*e*)

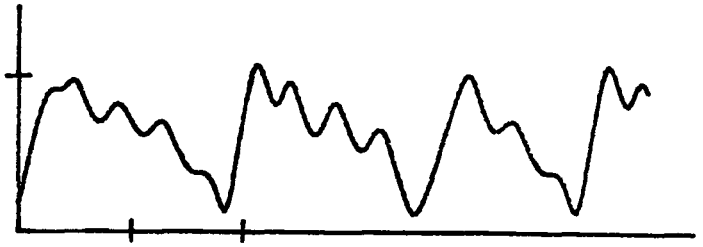

(*f*)

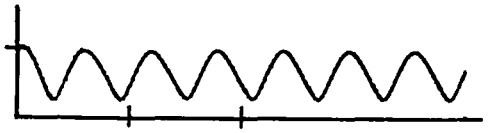

(*g*)

FIGURE 6. Various kinds of whirl phenomena seen as displacement versus time. Horizontal marks indicate time duration of 100 cycles at the operating frequency. Vertical marks indicate displacement of $0.1h_0$. (*a*) steady whirl, $h_0/R = 0.14$, $\omega/\omega_0 = 1.6$, $C = 0.28$; (*b*) periodic modulation, 0.14, 1.6, 0.17; (*c*) periodic modulation, 0.14, 1.73, 0.28; (*d*) periodic modulation, 0.14, 1.63, 0.28; (*e*) aperiodic modulation, 0.14, 1.53, 0.28; (*f*) aperiodic modulation, computation from modified Korteweg–de Vries equation ($E_1 = 0$), 0.14, 1.5, 0.30; (*g*) periodic modulation, computation from modified Korteweg–de Vries equation ($E_1 = 0$), 0.14, 1.6, 0.18.

6. Results

Observation of the behaviour of the system during a whirl run discloses many interesting phenomena. At operating speeds below some critical value there is no evidence of any motion other than the rotation of the centrifuge about its geometric axis. After this lower critical speed is passed, the system begins to whirl at a frequency other than the operating frequency. Further increase in operating speed leads to an increase in whirl amplitude, until at some operating speed the whirl amplitude reaches a maximum. Subsequent increases in operating speed result in a decrease in whirl amplitude, until finally the whirl disappears at an upper critical frequency and the bowl is again rotating about its geometric axis. The lower and upper critical frequencies define a region of operating frequencies in which the system is said to be unstable. The extent of the unstable region depends on the fluid load, fluid density and viscosity, external damping and resonant frequency. A report of the complete experimental study of the linear stability region will appear elsewhere. Here attention will be focused on some of the more interesting observations made during active finite-amplitude whirling motion.

Observation of the free surface during finite-amplitude whirl disclosed several phenomena which appear at different operating frequencies for a given fluid load, damping, and resonant frequency. Figure 2(*a*) is a photograph which clearly shows a 'hydraulic jump' across which the fluid depth changes suddenly from one value to another. Figure 2(*b*) illustrates a weaker hydraulic jump with undulations behind it. Figure 2(*c*) shows what appears to be a 'solitary' wave on the fluid surface. Numerically produced surface shapes have been computed and are in very good agreement with these observations. These will be presented in a separate publication.

Active whirl of three different types has been observed:

(i) steady whirl, i.e. whirl with essentially time-independent amplitude;

(ii) periodic time-dependent whirl during which the whirl amplitude varies in a reasonably periodic fashion, slowly modulating the high-frequency whirl oscillations;

(iii) aperiodic time-dependent whirl during which modulations occur that are clearly not periodic.

These features are illustrated by the traces obtained from the hot-stylus recorder of the whirl signal from one of the Kamen probes. Operating conditions are given for each figure. Steady whirl is exemplified by figure 6(*a*), whirl with periodic amplitude modulation is illustrated by figures 6(*b–d*). Finally a clear example of whirl with aperiodic amplitude modulation is shown in figure 6(*e*). Figures 6(*f*, *g*) show similar results from the numerical computation. Figure 6(*f*) in particular shows aperiodic behaviour similar to that in figure 6(*e*). These are both at the same operating conditions.

Results showing amplitude response are collected in figure 4. This shows amplitude versus operating frequency (Δ_0/h_0 versus ω/ω_0) at one set of operating parameters ($h_0/R = 0.14$, $(\nu/\omega_0 R^2)^{\frac{1}{2}} = 0.0015$, $c = 0.18$, $\mu = 0.032$). On this figure are shown the hydraulic jump calculation from §3, the results from the modified Korteweg–de Vries calculations from §4, and a set of experimental amplitudes taken from the hot stylus recorder. The experimental results are shown as a maximum and a minimum runout when the whirl is not steady. Different symbols are used to distinguish between periodic and aperiodic modulations. It will be observed that there is a noticeable lack of agreement between the theories and the experiment especially near the peak amplitude but that the qualitative agreement is good. The Korteweg–de Vries calculation shows a region of modulation to the right of the peak, as does the experiment, but does not have such a region on the left.

This work was partially supported by the Union Carbide Corporation, Nuclear Division, operators of the Oak Ridge Gaseous Diffusion Plant for the United States Department of Energy. Support was also obtained from the National Science Foundation under Grant No. MEA-8210341, by Ames Research Center during a sabbatical (T.S.L.), and by a grant from the University of Minnesota Computer Center.

REFERENCES

CHESTER, W. 1968 *Proc. R. Soc. Lond.* A **306**, 5.

HENDRICKS, S. L. & MORTON, J. B. 1979 *Trans. ASME* E: *J. Appl. Mech.* **46**, 913.

KOLLMANN, F. G. 1962 *Forsch. Gebiete Ingenieurwess.* B **28**, 115 and 147.

MILES, J. W. & TROESCH, B. A. 1961 *Trans. ASME* E: *J. Appl. Mech.* **28**, 491.

WHITHAM, G. B. 1974 *Linear and Nonlinear Waves*, chap. 13. Wiley.

WOLF, J. A. 1968 *Trans. ASME* E: *J. Appl. Mech.* **35**, 676.